Organic Electronics 36 (2016) 35–44

Contents lists available at ScienceDirect

Organic Electronics

journal homepage: www.elsevier.com/locate/orgel

Homologous binary mixtures and improved hole conduction of self-assembled discotic liquid crystals

Ammar A. Khan [a, *], Girish Rughoobur [b], Muhammad A. Kamarudin [a], Alessandro Sepe [c], James A. Dolan [a, d], Andrew J. Flewitt [b], Malik M. Qasim [a], Timothy D. Wilkinson [a]

[a] Centre of Molecular Materials for Photonics and Electronics, Department of Engineering, Electrical Engineering Division, University of Cambridge, 9 J.J. Thomson Avenue, Cambridge, CB3 0FA, UK
[b] Electronic Devices and Materials Group, Electrical Engineering Division, 9 JJ Thomson Avenue, Cambridge, CB3 0FA, UK
[c] Adolphe Merkle Institute, Chemin des Verdiers 4, CH-1700 Fribourg, Switzerland
[d] Cavendish Laboratory, Department of Physics, University of Cambridge, JJ Thompson Avenue CB3 0HE, Cambridge, UK

ARTICLE INFO

Article history:
Received 15 April 2016
Received in revised form
20 May 2016
Accepted 22 May 2016
Available online 31 May 2016

Keywords:
Discotic liquid crystals
Organic semiconductors
Molecular p doping
Self assembly

ABSTRACT

Discotic liquid crystals (DLCs) are considered promising materials for organo-electronic applications. Columnar alignment of DLCs leads to anisotropic charge transport with high charge carrier mobility. However, pure DLCs exhibit low intrinsic charge carrier density which limits bulk conductivity. This research studies the alignment and conductivity properties of small molecule triphenylene-based DLCs to develop hole transport layers for potential applications in organic semiconductor devices. Binary mixtures of homologous DLCs of the hexakis(n-alkyloxy)triphenylene series (HAT6 and HAT10) are formulated. Mesophase characteristics and columnar alignment of these mixtures are characterized using polarizing optical microscopy (POM) and differential scanning calorimetry (DSC). Alignment, orientation and order of columnar packing in the mixtures is studied using X-ray diffraction (XRD) and grazing incidence wide angle X-ray scattering (GIWAXS) measurements. It is identified that binary mixture formation strongly effects the columnar alignment in solution processed films. Furthermore, to increase charge carrier density in the DLC films a strong electron acceptor 2,3,5,6-tetrafluoro-7,7,8,8-tetracyanoquinodimethane (F4TCNQ) is added as a p-type dopant, followed by an extensive characterization of its doping effect. POM, DSC thermal scans, UV–visible spectroscopy, photo-luminescence spectroscopy (PL) and I-V measurements are utilized to characterize and establish the improvement of hole conduction in the doped films. It is observed that F4TCNQ-doped triphenylene DLC films exhibit two-fold increase in hole conductivity, making the materials highly relevant for charge transport applications.

1. Introduction

Discotic liquid crystals (DLCs) typically exhibit columnar mesophase characteristics, where the mesophase exists in a given temperature range [1]. DLCs were first discovered in 1977 by Chandrasekhar [2,3] while he was working with hexaesters of benzene. Since then, DLCs have been studied extensively from both fundamental and application perspectives [4–7]. The mesophases are typically comprised of disc-shaped molecules that form molecular columns due to phase segregation of the aromatic and aliphatic segments, in addition to π-π interactions between the poly-aromatic molecular condensed cores. Individual poly-aromatic molecules exhibit significant pi-conjugation, and overlap within well-aligned molecular columns have motivated significant efforts to realize their potential as self-assembled organic semiconductors [2,4,8–11].

Organic semiconductors have been an area of keen interest for several decades now, with some of the earliest successful investigations dating back to 1956 [12]. The possibility of having semi-conducting solution processed materials that can be easily and cheaply deposited at low temperatures to fabricate optoelectronic devices such as organic light emitting diodes (OLEDs) [13], organic solar cells [14–16] and field-effect transistors [17] is very appealing for industrial applications. The underlying physical

* Corresponding author.
E-mail address: aak46@cam.ac.uk (A.A. Khan).

http://dx.doi.org/10.1016/j.orgel.2016.05.027

principles that makes almost all types of organic semiconductors (polymeric and small molecule) possible is bond conjugation (alternating π-σ bonds), that leads to the splitting of molecular energy levels, to induce band-like energy levels: conduction (lowest unoccupied molecular orbital (LUMO)) and valence (highest occupied molecular orbital (HOMO)) [18].

DLC molecules typically have conjugated aromatic cores, with substituted alkyl-chains that induce liquid crystalline (LC) behaviour. Numerous different families exist based on varying polyaromatic cores, such as triphenylene [19], pyrene, porphyrin [20], phthalocyanine, and hexabenzocoronene [21]. The inter-molecular packing of DLC materials is important in determining the charge transport mechanism of the materials in optoelectronic applications. As an example, the distance between adjacent aromatic cores in the LC state of hexahexyloxytriphenylene (HAT6) is estimated to be about 3.5 A°, which is short enough to enable charge carrier hopping between molecules along the columnar axis. However, the intermolecular gap is too wide to favour band-like conduction [4,22]. Charge hopping (transport) is only favourable along the columnar axis and the alkyl chains then act as insulating spacers, leading to orientational anisotropy in the effective charge carrier mobility and conduction. This anisotropy has been measured previously [23] and can be imagined of as the self-assembly of molecular wires along the columnar direction, where the individual columns are insulated from each other through the alkyl sidechains. This intrinsic electrical conductivity anisotropy of columnar DLCs is potentially useful for device applications, but the key to proper utilization lies in the ability to control the orientation of the molecular columns in both the LC (liquid crystalline phase) and Cr (crystalline phase). Two of the most common orientations are described with respect to the columnar axis (director), either parallel (planar) (Fig. 1f), or perpendicular (homeotropic) (Fig. 1e) to the plane of the substrate.

It has been demonstrated that DLCs typically exhibit high charge carrier (typically hole) mobility [21,24], and an increase in the aromatic core size of the constituent molecules increases the charge carrier mobility. However, LC molecules with larger aromatic cores have higher LC to isotropic (I) transition temperatures, poor solubility, are less desirable for capillary filling through melt processing. In this study, we use triphenylene-based DLCs, that have a relatively small core size ($\Sigma\mu \approx 0.002$ cm^2 V^{-1} s^{-1} in the LC phase [21], with four fused benzene rings in the aromatic core). However, they demonstrate a low melting and clearing point, allowing low temperature melt processing.

One of the commonly utilized and highest performing small molecule for hole transport layer applications is 2,2′,7,7′-tetrakis-(*N*,*N*-di-4-methoxyphenylamino)-9,9'-spirobifluorene (Spiro-OMeTAD). It has recently been shown that Spiro-OMeTAD can be doped with dicationic Spiro salts to increase the material conductivity to ~1 × 10^{-1} S/m [25], up from conventional Lithium salt doped Spiro-OMeTAD that typically yielded conductivity of the order of ~1 × 10^{-3} S/m [26]. The highest value of hole mobility in doped Spiro film ever reported is of the order of 10^{-4} cm^2/Vs [27], this is in fact lower than the hole mobility in triphenylene HAT6 (10^{-3} cm^2/V) [21]. So, combined with the higher mobility, smaller molecular size, lower melting temperatures and higher control of alignment properties, there is significant motivation to improve the conductivity of triphenylene DLCs to yield competitive, and possibly better hole transport layers.

In this study we focus on both the alignment and conductivity of hexakis (n-alkyloxy)triphenylene DLC derivatives HAT6 and HAT10 in the plastic crystalline (Cr) phase [28]. As these materials crystallize at room temperature, understanding and controlling the alignment in the LC-Cr transition upon cooling is critical. Local defects at domain boundaries can trap charge carriers, leading to lower charge carrier mobilities [29]. Significant work has been

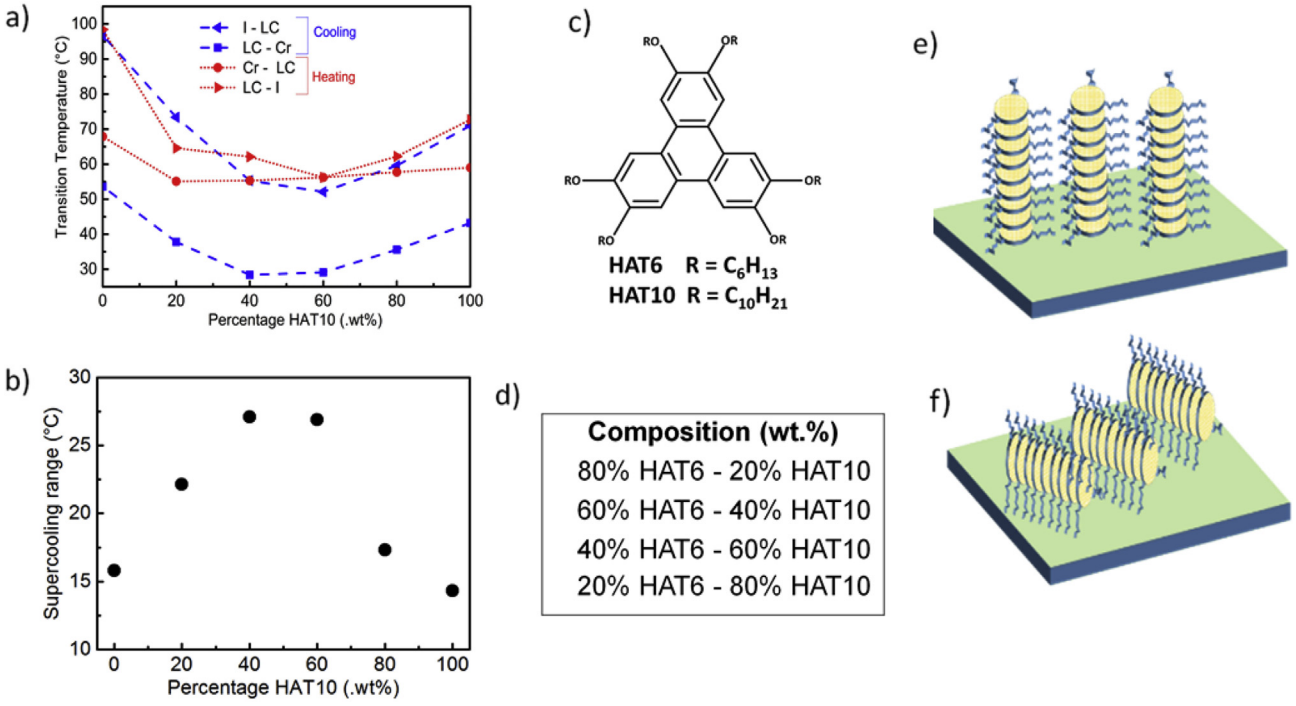

Fig. 1. Plots of phase transition temperatures of HAT6 - HAT10 binary mixtures on heating (red lines) and (b) cooling (blue lines), extrapolated from DSC thermal scans (5 ℃/min). (b) Illustrates the super-cooling effect in binary mixtures of HAT6-HAT10. Data points have been quantified by the difference between the crystallization (LC-Cr) and melting (K-LC) transitions. (c) illustration of the chemical structure of HAT6 and HAT10. (d) Summary of the binary mixture compositions prepared using HAT6 and HAT10. (e), (f) Schematics of the two most common alignment directions of columnar DLC phases, with (e) homeotropic alignment, director normal to substrate, and (f) planar alignment, with columnar director parallel to substrate. (For interpretation of the references to colour in this figure legend, the reader is referred to the web version of this article.)

performed on controlling the alignment of DLCs, including zone-casting [1], chemical substitution (partial chain perfluorination [30]) and the use of sacrificial polymer layers to induce the desired columnar alignment [31]. We present a relatively simple approach that involves the preparation of binary mixtures that utilize the same core, but varying aliphatic chain length to change columnar alignment. It is postulated that the combination of a larger (HAT10) and smaller (HAT6) molecule results in the formation of hybrid molecular columns that contain both constituents and modify the crystallization behaviour of the intrinsic materials.

Long-range ordering of molecular columns predominantly affects charge carrier mobility by maximizing π-π overlap. However, increasing the conductivity of DLCs is another engineering challenge as it requires ordering (mobility) as well as a high charge carrier density. DLCs, typically have large band gaps (>3.5 eV [5,32]) and this results in low intrinsic charge carrier concentration. Several studies have been performed to increase the conductivity using oxidizing agents and electron acceptors/donors [9,33–35]. In this study, we have utilized 2,3,5,6-tetrafluoro-7,7,8,8-tetracyanoquinodimethane (F4TCNQ) as a small molecule dopant for DLCs HAT6 and HAT10. F4TCNQ is widely recognized as a molecular p-type dopant due to its high electron affinity [36–38]. It is observed that the doping leads to the formation of a charge transfer complex, that results in an increase in the electrical conductivity of the intrinsic materials by almost two orders of magnitude. This opens up the possibility of using these self-assembled DLC materials in optoelectronic device applications.

2. Materials, mixture formulation and cell fabrication

2,3,6,7,10,11-Hexakishexyloxytriphenylene (HAT6) (SYNTHON Chemicals) and 2,3,6,7,10,11-hexakisdecyloxytriphenylene (HAT10) (SYNTHON Chemicals) DLCs were used as received. 2,3,5,6-Tetrafluoro-7,7,8,8-tetracyanoquinodimethane (F4TCNQ), (Sigma Aldrich) was utilized as an organic p-type molecular dopant. Binary mixtures of HAT10 and HAT6 were prepared with different weight percentage (wt%) (Fig. 1d). To ensure homogeneous mixing, toluene (Fisher Scientific) was used as a solvent, and subsequently evaporated. The mixtures were doped with F4TCNQ at concentrations of 0.1 wt%, 1 wt% and 5 wt%. Toluene was again used as a solvent to ensure homogenous mixing. All materials were used without further purification.

To prepare thin DLC spin-coated films on ITO-glass for current-voltage (I-V) measurements, the mixture under consideration was dissolved in anhydrous chlorobenzene (Sigma Aldrich) at a concentration of 15 mg/ml (for ≈ 120 nm eventual film thickness, measured using ellipsometry) and 175 mg/ml (for ≈ 1.15 μm thick films), followed by a two-stage spin-coating (1000 rpm for 30 s and 2000 rpm for 2 min). Top contacts were made by either evaporating 100 nm of gold, or sputtering Nickel (Ni) (≈200 nm) directly on top of the DLC film using a shadow mask (0.5 cm^2) to make the second contact.

3. Experimental methods

A polarizing optical microscope (POM) (Olympus BX-60) was used to visualize the textures of the doped and un-doped DLC films. A spectrometer (Ocean Optics USB-2000) was used to record absorption spectra of K DLC films in the visible spectrum (400–700 nm), and a UV–Vis (300–1100 nm) spectrometer (Agilent 8453) was used to record spectra in solution. A heating stage and temperature controller (Linkam TMS 94) integrated with the POM was used to monitor phase transitions. Most of the initial POM and current-voltage (I-V) analysis was performed in capillary filled 9 μm indium tin-oxide (ITO) coated glass cells. The materials were capillary filled into the cells in the isotropic phase.

Differential scanning calorimetry (DSC) (Mettler Toledo 823^e) was used to accurately determine phase transitions with a cooling and heating rate of 5 °C/min. I-V measurements were performed using a Keithley 4200-SCS parameter analyzer. Photo-luminesence (PL) measurements were performed using a gated intensified CCD camera system (Andor iStar DH740 CCI-010) connected to a grating spectrometer (Andor SR303i). Femtosecond excitation laser pulses with photon energy of 3.1 eV, pulse length ~100 fs and fluence 2 μJ/cm^2 were utilized. PL was obtained by temporally averaging the emission in the detection software (exposure time 0.2 s, 5 μs gate width). Tapping mode atomic force microscopy (AFM, Model 5400 Scanning probe Microscope, Agilent Technologies) was performed to study the topology of spin-coated DLC films on a 300 nm SiO_2 on Si substrate. The crystalline nature of the samples was studied using a Brucker D8 x-ray diffractometer (XRD) $\lambda = 1.5418$ Å. Symmetric θ-2θ scans of the samples over a narrow range from $2\theta = 2.5^\circ$ to $2\theta = 5^\circ$ were used to study the columnar packing. In addition, grazing incidence wide angle X-ray scattering (GIWAXS) was used to further analyze the order and orientation of the molecular columns. GIWAXS measurements were performed at beamline D1, at the Cornell High Energy Synchrotron Source (CHESS) at Cornell University in Ithaca, NY, U.S.A. The wavelength was 1.17 Å.

4. Results and discussion

Binary mixtures of HAT6 and HAT10 were prepared in different wt% of the two components (Fig. 1d). Phase transition temperatures measured using DSC measurements of the mixtures are presented in Fig. 1a, where the phase transition temperatures on heating and cooling are illustrated. It can be seen from the phase transition temperatures on cooling (Fig. 1a, blue lines) that there is a decrease in the LC-Cr transition temperatures upon binary mixture formation. The LC phase is found to exist at temperatures as low as 30 °C in 40% HAT6 - 60% HAT10, which is very low when compared to the LC-Cr transition of pure HAT6 that occurred at 54 °C. However, the Cr-LC phase transition temperatures on heating do not follow the same trend (red line Fig. 1a). It can be seen that the Cr-LC temperature is almost constant throughout the mixtures on heating (≈55 °C). This is evidence of supercooling (depression of LC-Cr transition on cooling), which is common in LC mesophases, and was reported previously by Boulingand et al. in their work with triphenylene DLCs [39]. Fig. 1b illustrates the extent of supercooling plotted against the mixture compositions. It was found that while the LC phase can be accessed at lower temperatures in the binary mixtures on cooling from isotropic, this drop is not replicated upon heating, such that the drop in crystallization temperature observed on cooling and is not a true lowering of the melting point in eutectic mixtures.

POM textures of the mixtures in drop-cast DLC thin films in a cover-slip configuration without any additional alignment layers are summarized in Fig. 2 and Figure S1. The optical texture of HAT6 in the LC phase (Fig. 2a) demonstrates large areas of dark platelets where the columns are aligned homeotropically, and bright fan-like/spherulite regions that are indicative of planar alignment (as birefringence is minimum for light propagation parallel to the columnar director (homeotropic), and maximum perpendicular (planar)). On cooling to the plastic Cr state (Fig. 2b), it can be seen that the texture is very bright under crossed polarizers, with numerous micron-sized coloured domains forming on crystallization. This is due to a loss of the homeotropic (optically isotropic) alignment, to disordered/tilted columns on crystallization that increase the effective birefringence, and manifests as a bright texture. A similar change in texture is also seen in HAT10 during the

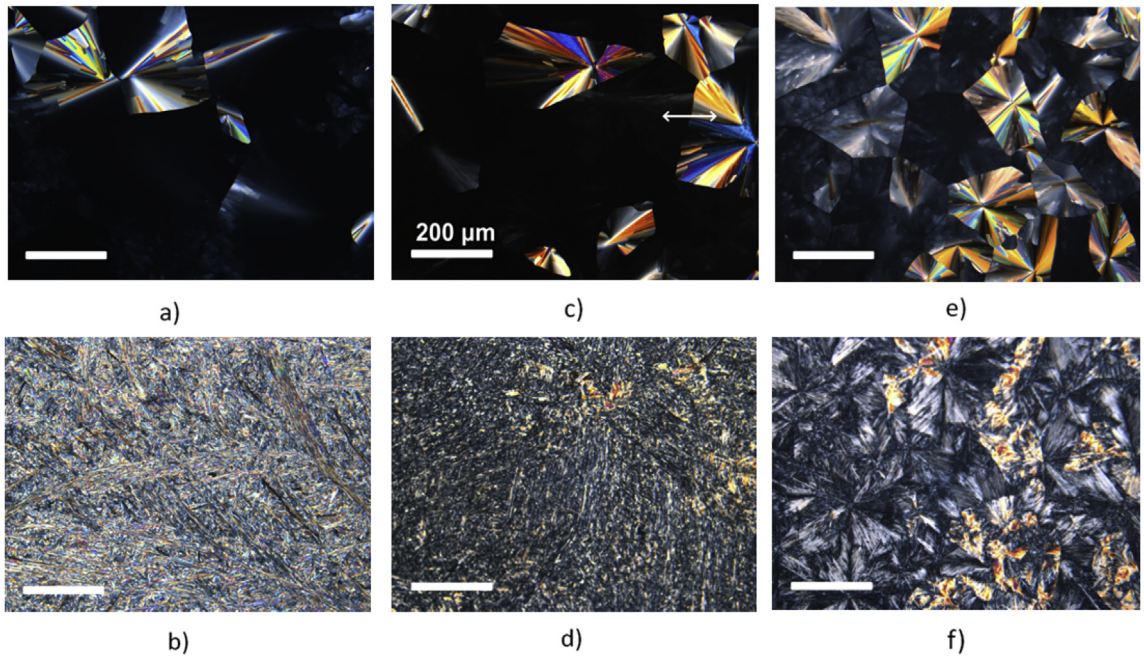

Fig. 2. a-f POM micrographs of drop-casted DLC thin films in a cover-slip configuration on cooling from isotropic, recorded under crossed polarizers. Textures of HAT6 at (a) 98 °C, columnar phase and (b) 55 °C, crystalline phase. The optical texture of the longer side-chain HAT 10 in the columnar, 74 °C (c) and crystalline, 45 °C (d) phase. The change in morphology on phase transition from LC-Cr in the binary mixture of 40% HAT6 – 60% HAT10 can be seen in (e) LC, 55 °C and (f) Cr, 34 °C.

transition from the LC (Fig. 2c) to the Cr phase (Fig. 2d). For the binary mixture 40% HAT6 - 60% HAT10, the POM results indicate a different response. It can be seen that significant features of the initial columnar domain structure are preserved between the transition from the LC (Fig. 2e) to the plastic Cr phase (Fig. 2f). Figure S1 illustrates POM results for the other binary drop casted HAT6 & 10 mixtures from Fig. 1d.

POM textures of spin coated films are shown in Fig. 3a-c. The films are crystalline and have an air interface at the top. HAT6 forms a distinct fan-like spherulite texture with individual domains that stretch across 200–300 μm. The texture of HAT6 (Fig. 3a) can be classified as a predominantly planar alignment with the hexagonal packed columns lying parallel to the substrate. HAT10 (Fig. 3b) illustrates a similar texture to HAT6, however, in the case of HAT10 the domains are much smaller ~≤30 μm, and the alignment is predominantly planar.

In the case of the mixture 40% HAT6-60% HAT10 the spin-coated film (measured to be 2 μm using optical interference) shows large areas with low birefringence, amongst areas of high birefringence. The birefringence of the dark regions however (marked by green outline) remains low on rotation of the sample under crossed polarizers. The seemingly optically isotropic texture of the inherent birefringent materials can be explained either as large domain homeotropic alignment (which could be very useful for out-of plane applications), or a disordered crystalline state where any birefringence is averaged out leading to a dark texture. Atomic force microscopy (AFM) analysis of the films (Fig. 3d-f) showed that the binary mixture had a more level topography as compared to HAT6 and HAT10. AFM analysis of spin-coated films of HAT6 (Fig. 3d) and HAT10 (Fig. 3e) displayed a general waviness of at the surface, whereas the binary mixture (Fig. 3f) did not exhibit such waviness, and instead demonstrated a very planar interface. The surface roughness of all films was actually very similar. The AFM profiles combined with the DSC data show that the two components of the binary mixtures are compatible with each other, forming very uniform films in a single step deposition process.

In order to understand the inherent columnar alignment better, XRD analysis and in-plane and out-of-plane conductivity measurements were performed. XRD data is summarized in Fig. 3g where it can be seen that all the films showed a diffraction peak within a 2θ angular range of 3–5°, corresponding to inter-columnar spacing, as concluded in previous similar studies [40]. The spacing can be calculated to be approximately 2.03 nm for HAT6, 2.54 nm for HAT10 and 2.57 nm for 40% HAT6 - 60% HAT10. The peak positions for HAT10 and HAT10-6-3 almost to correspond to the same inter-columnar distance. The results are consistent as HAT6 which is the smallest molecule has the smallest inter-columnar distance, and HAT10 shows a relatively larger inter-columnar distance through a smaller diffraction angle. However, only one peak was seen in XRD data of the binary mixtures corresponding to the spacing of the HAT10 columns leading to a picture of intercalated molecular columns that are as wide as HAT10 but contain both HAT6 and HAT10. So, in order to study the columnar structure at higher resolution, grazing incidence wide angle X-ray scattering (GIWAXS) was performed. The results are summarized in Fig. 3h,i. Scattering profiles corresponding to planar alignment can be seen in Fig. 3h, and the contributions from homeotropic alignment of the columns are seen in Fig. 3i. The GIWAXS data has a higher resolution and sensitivity than the XRD data and, unlike the XRD data, two separate scattering peaks were observed in the binary mixture corresponding to HAT6 (20.16 Å) and HAT10 (24.44 Å).

Conclusion drawn by analyzing the GIWAXS scattering profiles do not support the hypothesis that the dark regions seen in Fig. 3c are regions of improved homeotropic alignment as the scattering peaks corresponding to homeotropic alignment (Fig. 3i) are smaller in intensity relative to the planar alignment peaks and do not show significant enhancement when compared to the homeotropic scattering peaks of HAT6 and HAT10. However, by looking at the third order Bragg reflections in the planar alignment profiles, it can be seen that the binary mixture exhibits sharper higher order peaks that are indicative of long-range ordering of the planar oriented backbone. This was further confirmed by in-plane conductivity

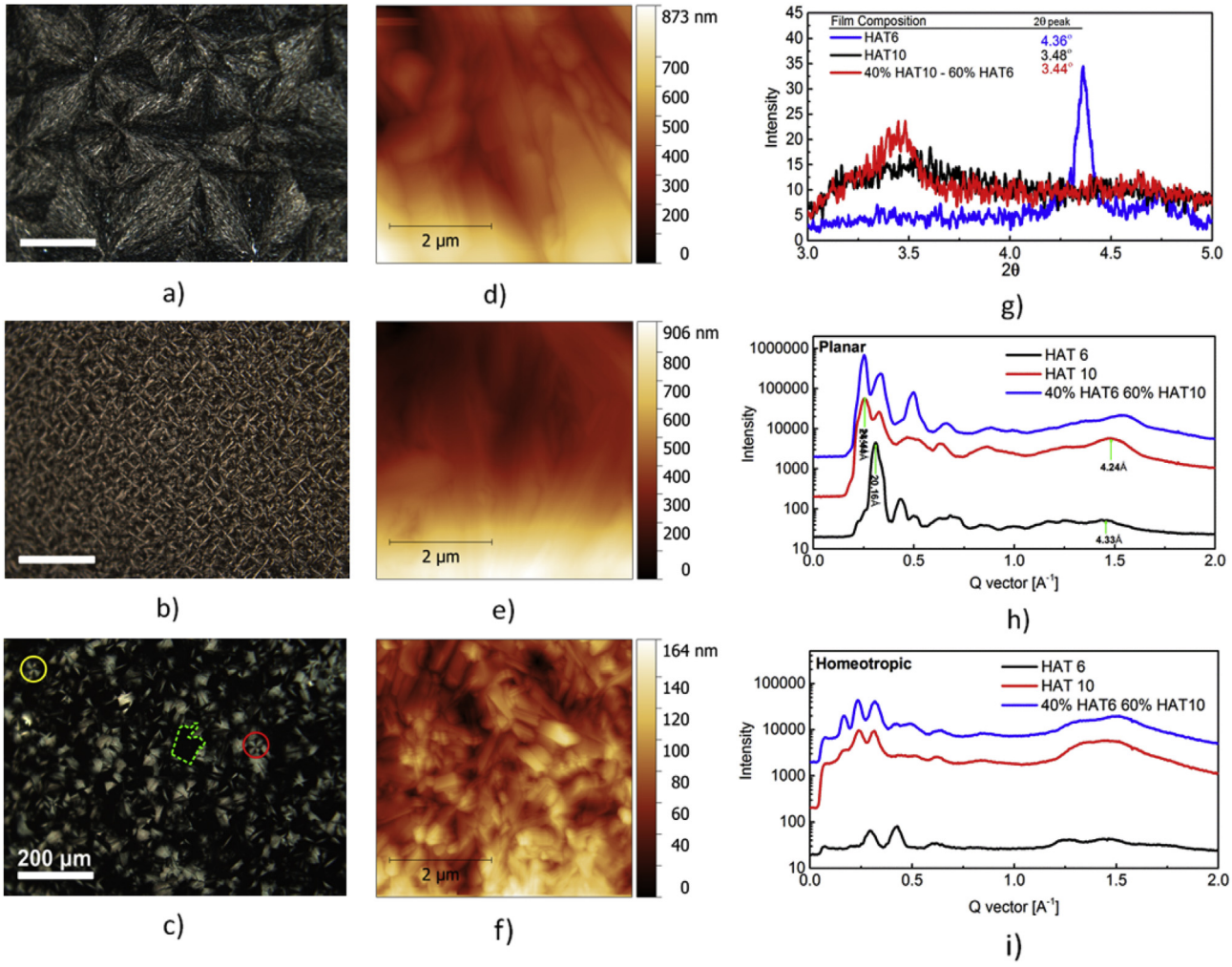

Fig. 3. POM, AFM and X-Ray analysis of spin-coated 175 mg/ml films of HAT6, HAT10 and 40% HAT6 - 60% HAT10 on 300 nm SiO_2 on Si substrates. a-c POM micrographs (a) HAT6, (b) HAT1 and (c) 40% HAT6 - 60% HAT10. (d–f) Surface topology of the spin-coated films for (d) HAT6, (e) HAT10 and (f) 40% HAT6 - 60% HAT10. X-Ray data of the films is summarized in (g) XRD data the DLC materials, and (h), (i) illustrates the GIWAXS scattering data of the films corresponding to (h) planar and (i) homeotropic columnar alignment of the DLC films.

measurements (Fig. 4b) where the binary mixture demonstrates higher in-plane conductivity that HAT10. In summary, it can be seen that binary mixture formation strongly affects the columnar alignment and packing, and in the case of a 40% HAT6 – 60% HAT10 mixture we seem to have a columnar phase with large optically isotropic domains.

Alignment and columnar packing strongly affect charge carrier mobility. However, in order to compete with state of the art amorphous organic hole transport layers it is important to be able to increase the macroscopic electronic conductivity of the aligned films. The electrical conductivity of the DLC films was initially probed using I-V measurements in an ITO-ITO electrode configuration. In the case of films of pure HAT6, HAT10 and their binary mixtures that were 5 μm and thicker (tested in capillary filled cells), it was not possible to measure any DC current (<10 nA) at fields as high as 6 V/μm.

Fig. 4a illustrates the I-V curves for HAT6, HAT10 and a 40% HAT6 - 60% HAT10 binary mixture in out-of-plane ITO-DLC-Au test devices with the DLC film thickness measured to be ≈ 1.15 μm using interference and a profilometer. For the case of very thin films in Fig. 4a, it was possible to extract a measureable current, and conductivity of HAT6 can be approximately calculated to be (3×10^{-5} Sm^{-1}). However, for most opto-electronic devices it would be desirable to have a higher electrical conductivity with charge carrier transport being supported by thicker films (especially in the case of capillary-filled films from a device applications perspective). For the case of melt-processed HAT6 in ITO-ITO test devices, the electrical conductivity in 9 μm cell is estimated to be ≈ 2.4×10^{-11} Sm^{-1}, which is too low for any electronic device applications. The same was found to be the case for HAT 10 and the binary mixture HAT10-6-3.

Subsequently, in order to improve conductivity p-type doping of the HAT6, HAT10 and their binary mixtures was performed to increase the charge carrier concentration. F4TCNQ is a strong electron acceptor, with a (LUMO) level at −5.2 eV (vacuum). Previous cyclic voltammetry study on HAT6 [32] has estimated a (HOMO) level at −5.38 eV. Doped mixtures of HAT6 were prepared with F4TCNQ as 0.1 wt%, 1 wt% and 5 wt%. The absorption spectrum of crystalline 9 μm thick F4TCNQ-doped HAT6 films in ITO-ITO sandwich cells (Fig. 5a) shows interesting characteristics (for UV–Vis spectra of pure HAT6 and 1 wt% F4TCNQ doped in solution form, refer to Figure S4). There is a clear absorption shoulder around 575 nm that is not present in pure HAT 6. This absorption peak is shown to get higher with increasing dopant concentration. It is postulated that

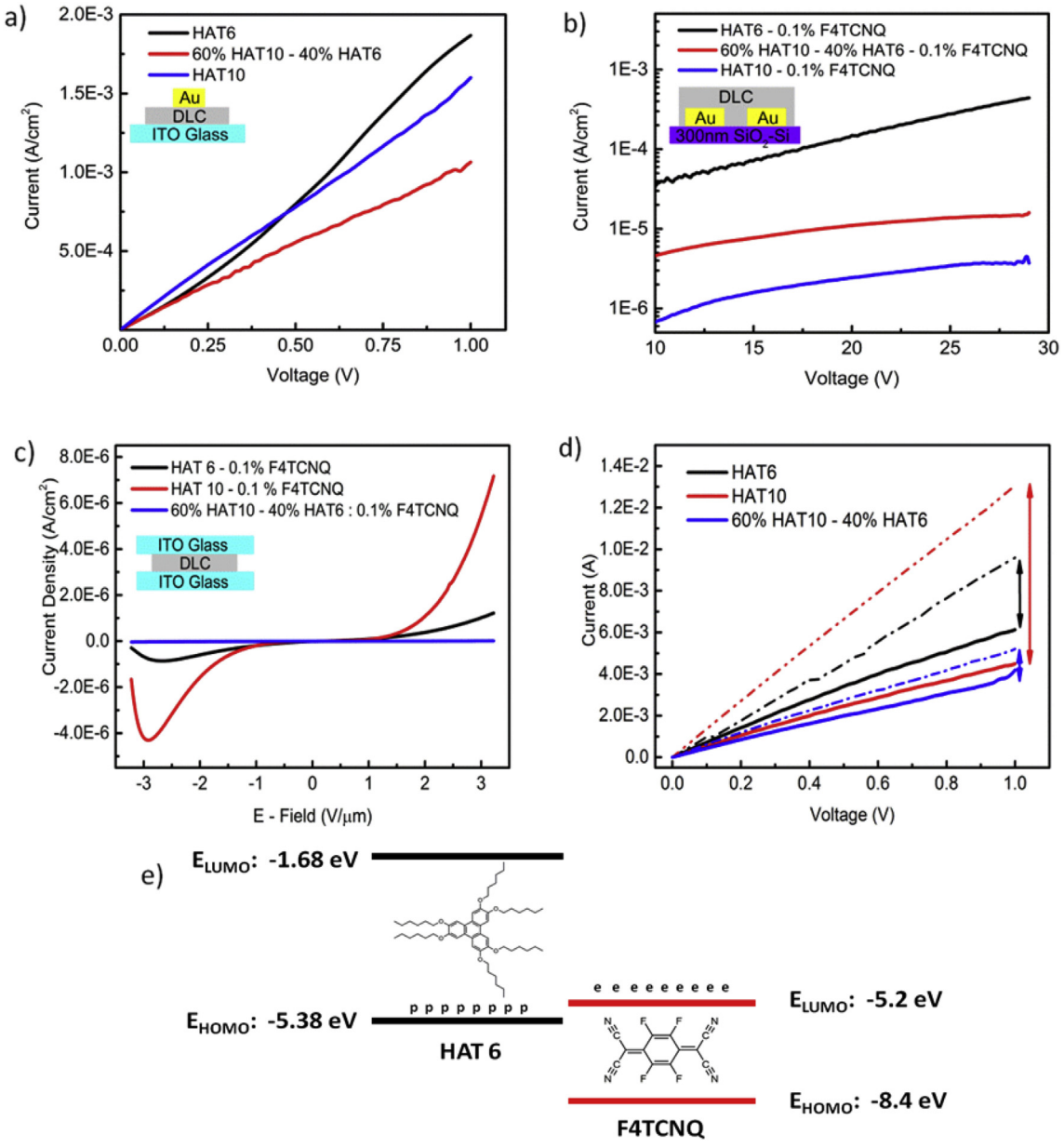

Fig. 4. (a) I-V curves of ≈1.15 μm thick DLC in Gold (anode)-DLC-ITO (cathode) sandwich devices, with films of intrinsic DLCs. (b) IV curves of 0.1 wt% doped spin-coated DLC films measuring the in-plane conductivity using gold electrode with a 10 μm gap and 0.8 cm channel length (c) IV curves of 0.1 wt% F4TCNQ-doped 9 μm DLC films in ITO-ITO sandwich cells. (d) IV curves of ≈120 nm thick intrinsic (solid lines) and 0.1 wt% F4TCNQ-doped (dashed lines) DLCs in a Ni (anode) – DLC – ITO (cathode) test cell geometry. (e). An illustration of the relative energy levels of HAT6 and F4TCNQ d.iii [32]' [41]. (For interpretation of the references to colour in this figure legend, the reader is referred to the web version of this article.)

this peak is indicative of the formation of a charge transfer complex between the dopant and DLC molecules, and this phenomena is similar to what has been reported on p-type molecular doping of other similar small molecules [26,36,38]. This result is very encouraging, as it proves that these materials are being successfully doped as p-type materials, even though there is a slight mismatch between the energy levels of the dopant and host material. Fig. 5b illustrates the change in absorption characteristics as a function of temperature for a 1 wt% F4TCNQ-doped HAT6 9 μm thick sample. At 40 °C, the absorption spectrum contains contributions from both Mie-scattering (due to disorder in the texture) and electronic transitions. However, it is important to note here that at 120 °C the material is isotropic, so any absorption seen in that case is due to electronic excitations in the charge transfer complex.

DSC measurements of the doped mixtures (Supplementary Figure S2) showed increasing shift from pristine HAT6 on increasing doping concentration. Fig. 5d illustrates the LC-Cr transition on cooling from isotropic in the doped mixtures. A fall in the melting point was observed, and the DSC results confirmed homogeneous mixing and chemical compatibility of the dopants in the host LCs. PL measurements of intrinsic HAT6 and 0.1 wt% F4TCNQ-doped HAT6 (Fig. 5c) showed enhanced emission around 575 nm consistent with the energy levels of the charge transfer complex, and corroborate the absorption spectra. POM of doped HAT6 mixtures (Fig. 6) in the Cr state illustrate a decrease in domain size on increase in doping concentration, corresponding to increasing disorder due to added impurity and nucleation sites. The DSC and temperature controlled POM of HAT6 up to 1 wt% doping

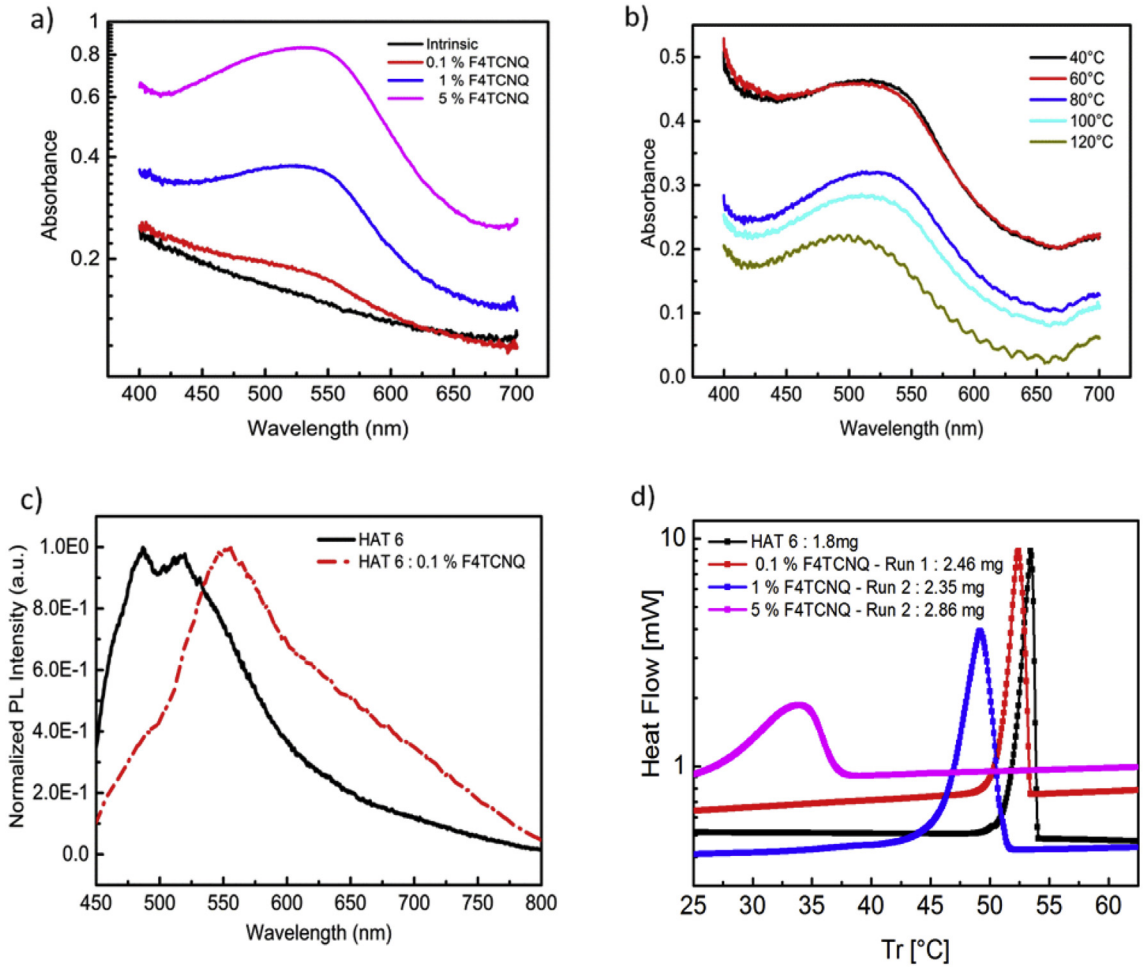

Fig. 5. (a) Visible light absorption spectrum of doped HAT6 films, with an absorption shoulder around 575 nm, corresponding to a F4TCNQ-DLCs charge transfer complex, in the Cr state (25 °C). (b) Changes in the absorption spectrum of 1% F4TCNQ-doped HAT6 as a function of temperature (Cr-LC-I). (c) PL emission spectra of intrinsic and 0.1% wt.% doped HAT6. (d) Variation in the LC-Cr phase transition of intrinsic and doped HAT6 on cooling, measured using DSC.

are reasonably similar, with only minimal shifts in phase transition temperatures and optical textures. The 5 wt% mixture however, exhibited a large bi-phasic (LC-I) region on heating, with a strikingly different texture under crossed polarizers. Optical micrographs corresponding to spin-coated thin films of the doped DLC films (Supplementary figure S3) also illustrate increasing crystallization on doping.

I-V measurements of doped HAT6 mixtures were performed to quantify and compare the effect of p-type doping on conductivity properties. ITO-LC-ITO test cells were prepared with (5 μm, 9 μm and 20 μm) film thickness and Ni-LC-ITO test devices were prepared with ≈120 nm thick spin-coated LC films.

Fig. 4c illustrates the I-V curves of 9 μm thick 0.1 wt% F4TCNQ-doped HAT6, HAT10 and 40 % HAT6 - 60 % HAT10 mixtures, and the I-V curves in the Ni-LC-ITO architecture can be seen in Fig. 4b. In both cases, it is clear that doped HAT10 has the highest conductivity, whereas of the un-doped materials (Fig. 4a,b) HAT6 exhibits higher conductivity. This is rather surprising as it has longer insulating alkyl chains and charge carrier mobility has been shown by time-of-flight studies to decrease in triphenylene DLCs with increasing chain length [24]. 0.1 wt% F4TCNQ doped binary mixture 40% HAT6 - 60% HAT10 exhibits relatively lower out-of-plane conductivity, which is consistent with the hypothesis that the dark regions Fig. 3c are not indeed homeotropically aligned. However, as predicted by the GIWAXS analysis the in-plane conductivity of the binary mixture (Fig. 4b) is higher than HAT10.

The effect of increasing dopant concentration in capillary filled 9 μm thick HAT6 films can be seen in Fig. 7 a. There is a significant initial increase in charge conduction from intrinsic to 0.1% doped HAT6, which is very encouraging since it signifies an increase of conductivity by at least two orders of magnitude in the capillary filled 9 μm films on 0.1 wt% doping. Furthermore, the 1 wt% doped mixture illustrates an improvement over the 0.1 wt% doping, in both relatively thick (Fig. 7a) and thin (Fig. 7b) DLC films. 5 wt% doped mixtures of HAT6 however, illustrate a decrease in conductivity, in both 9 μm and thinner ≈120 nm films. This is interesting for two reasons, as firstly it points towards a decrease in charge carrier mobility due to dopant induced scattering and defects in the DLC morphology. Secondly it reinforces the claim that charge carrier transport in doped films is in fact due to electrons and holes (holes in this case) and not due to ionic migration of the F4TCNQ molecules, since if that was the case then increasing dopant concentration would have increased the measured conductivity even further in the 5 wt% doped mixture. However, the authors suggest further studies that look at Hall effect and impedance spectroscopy measurements to further investigate the mechanism of conduction in these p-type doped DLC films.

It can be seen that the calculated effective conductivity (using a linear resistive mode at a given I-V point) is much higher in the ≈120 nm thick Ni-DLC-ITO devices (Fig. 7b). This can be attributed

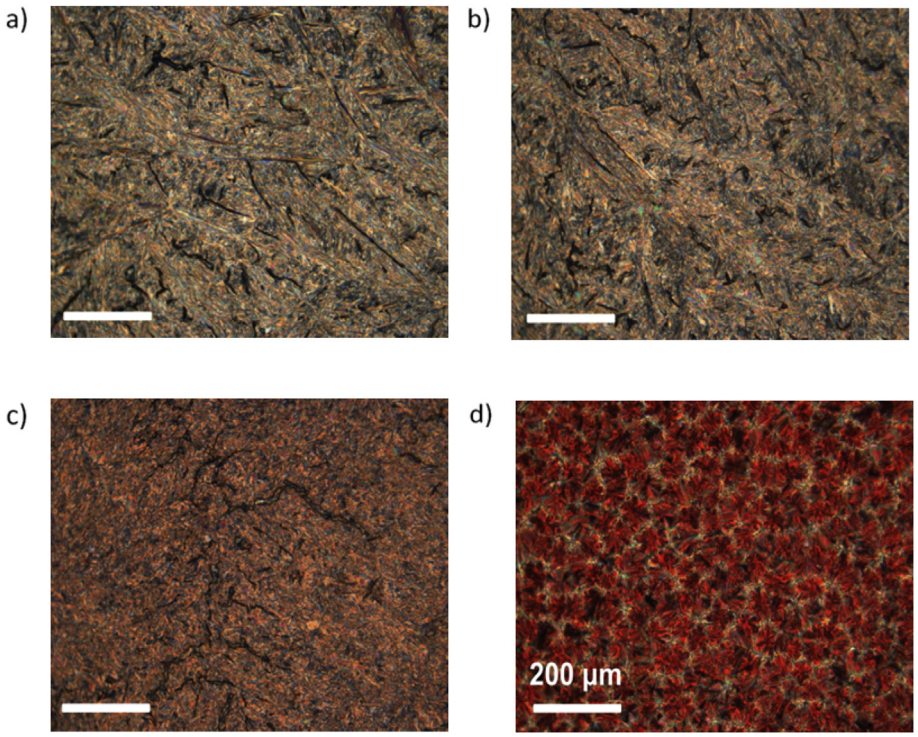

Fig. 6. POM of doped HAT6 textures at 25 °C, Cr phase. (a) Intrinsic HAT6, (b) 0.1 wt% F4TCNQ-doped, (c) 1 wt% doped, and (d) 5 wt% F4TCNQ doped HAT6.

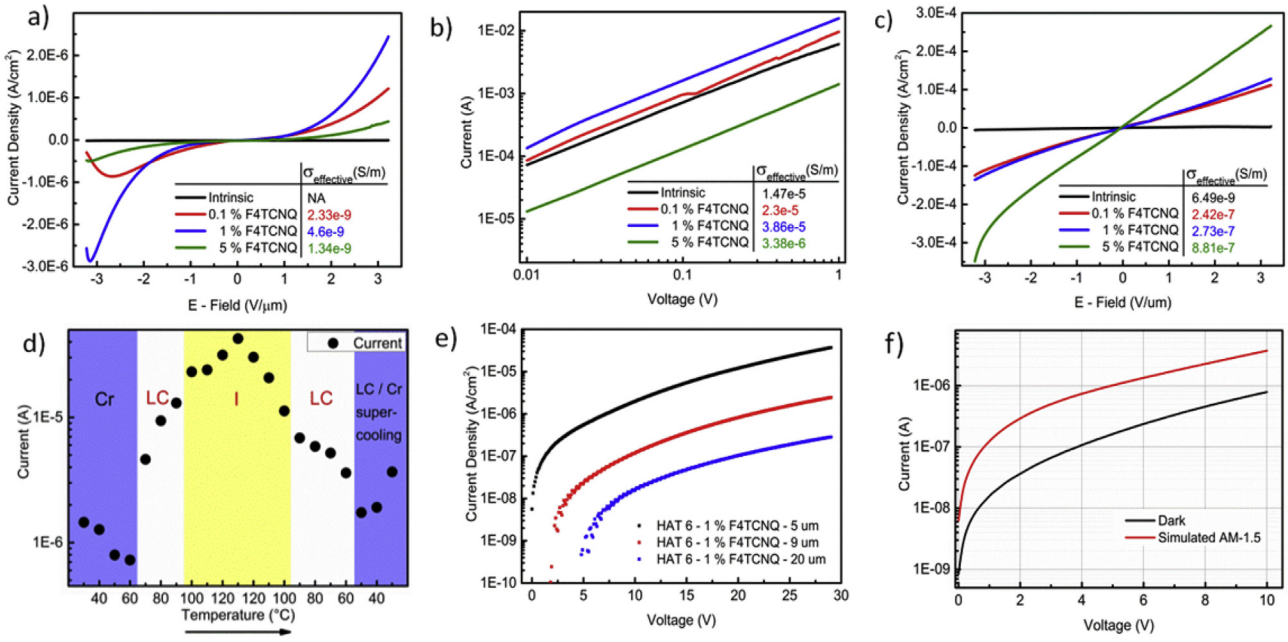

g)

Mixture	Effective Mobility ($cm^2/(V.s)$) 5 µm	9 µm	20 µm
HAT6 - 0.1 % F4TCNQ	7.55E-6	3.11E-6	8.25 E-6
HAT6 - 1 % F4TCNQ	9.32E-6	3.24E-6	7.64E-6

Fig. 7. (a) I-V curves on doped HAT6 films in 9 µm ITO-ITO cells at 30 °C, Cr phase (inset; estimated conductivity at 3 V/µm using a simple resistor model, s = d/(RA), where R = V/I, d = 9 µm and A is the overlap area of each device). (b) ≈120 nm doped DLC HAT6 films in a Ni-DLC-ITO architecture. (c) The doped DLC films are heated to isotropic, and I-V measurements performed on in 9 µm ITO-ITO cells at 180 °C. (d) Current measured for 0.1% doped F4TCNQ HAT6 at a field magnitude of 3 V/µm, as a function of temperature, in the I, LC and Cr phase. (e). I-V curves of a 1 wt% doped HAT6, illustrating the effect of thickness of the films in ITO-ITO capillary filled sandwich cells (25 °C). (f) Variation of the IV characteristics of a 1 wt% doped DLC 9 µm film in ITO-ITO cells in dark and simulated AM 1 1.5 1 sunlight conditions. (g) Table summarizing the effective charge carrier mobilities in 0.1 wt% and 1 wt% F4TCNQ-doped HAT6 films in ITO-ITO cells.

to better electrode contact (sputtered Ni on spin-coated LC), improved hole injection (higher Ni work function as compared to ITO) and higher effective hole mobility in the thinner films due to the presence of fewer grain boundaries that block charge transport. The mixtures were heated to record the I-V characteristics as a function of temperature in different phases. The I-V curves of the doped HAT6 mixtures in 9 μm ITO-ITO cells in the isotropic state are illustrated in Fig. 7c. It can be seen that compared to the case in the Cr phase (Fig. 7a) there is significantly higher conduction in the isotropic state. It is postulated that the increase in conductivity in the isotropic state is due to a reduction in scattering and improved charge transfer through the medium. The increase in conductivity was found to be reversible, and Fig. 7d demonstrates the effect of measured current at an applied E-field of 3 V/μm on a 0.1 wt% F4TCNQ-doped HAT 6 sample. It can be seen that each phase transition Cr-LC, followed by LC-I is accompanied by an increase in conductivity by an order of magnitude. This is reversible, and cooling from the I state was found to reverse the conductivity to previous levels.

To estimate the extrinsic hole mobility in the doped HAT6 films, a space charge limited current (SCLC) model was used to fit I-V curves in ITO-ITO sandwich cells. Based on the near quadratic relationship between current density and voltage at higher electric field magnitudes in Fig. 7a,e, the Mott-Gurney equation [42] is utilized; an average value of $\varepsilon_r = 2.61$ (0.1 wt%) and $\varepsilon_r = 2.82$ (1 wt% doped) is used as the average relative dielectric permittivities (based on capacitance data before and after filling sandwich cells).

$$J_{est} = \frac{9}{8}\varepsilon_0\varepsilon_r\mu\frac{V^2}{L^3} \quad (1)$$

Similar analysis have been reported on organic semiconductor (Spiro-MeOTAD) [27], and polymer [43] films. The measured I-V response was fit to equation (1) to estimate an effective mobility for 0.1 and 1 wt% doped 9 μm films in ITO-ITO sandwich cells, Figure S5 gives an example of the fit in the case of a 5 μm 0.1 wt% F4TCNQ doped sample. It was very interesting to note from Fig. 7g that the calculated mobility values for a given thickness are comparable for the two doping concentrations. Within the limitations of the model, this points towards minimal dopant induced disorder and hole scattering in the doped DLC films. Differences in the magnitude of estimated mobility across varying cell thickness can be associated with the conductivity anisotropy of DLCs, which makes conductivity heavily dependent on the alignment of the Cr phase.

It is observed that the addition of F4TCNQ to HAT6, HAT10 and their mixtures leads to an increase in conductivity of capillary filled and spin-coated films. Hole transfer from the HOMO level of the host DLC to the LUMO of F4TCNQ results in an increase in 'free' carrier concentration in the films.

However, in the interest of hole transport applications in photovoltaic devices, it is important to establish that the increase in measured conductivity is predominantly due to hole conduction and not the motion of ions/salts. The I-V characteristics presented in Fig. 7a (which show compatibility with the SCLC model), the decrease in measured conductivity of K films going from 1 wt% to 5 wt% doping (Fig. 7a,b), and the corresponding increase in films in the isotropic phase (Fig. 7c) all support the hole nature of conduction rather than ionic. Furthermore, I-V characteristics under dark and light (Simulated AM 1.5) conditions (Fig. 7f) show that increased photo-induced charge carrier concentration corresponds to an increase in measured conductivity, whereas the motion of salts/ions should be light independent. Using the above evidence, it is hypothesized that the predominant nature of conduction is indeed hole conduction, making these materials suitable for charge transport layer applications.

5. Conclusion

Binary mixtures of HAT6 and HAT10 that share the same aromatic core but different aliphatic chain lengths were characterized. Phase transitions of binary mixtures of HAT6, HAT10 were analyzed, and significant depression of the crystallization temperature on cooling was measured in binary mixtures, however significant super-cooling was identified in the mixtures and the depression was not replicated on heating. POM showed large domains of low birefringence (optically isotropic) in the crystalline phase in a 40% HAT6 - 60% HAT10 mixture that could either be explained by homeotropic alignment or disordered texture. X-ray analysis was performed, and XRD data showed that the columnar spacing can be calculated to be approximately 2.03 nm for HAT6, 2.54 nm for HAT10 and 2.57 nm for 40% HAT6 - 60% HAT10, where the column width is dominated by the larger constituent molecule in the binary mixture. However using GIWAXS scattering analysis it was later confirmed that the individual molecules in the binary mixtures form distinct columns as two peaks were observed. In addition, the x-ray scattering data did not show significantly increased homeotropic alignment in the binary mixtures, however the in-plane alignment and conductivity was improved over that of HAT10.

Furthermore, the electronic conductivities of the HAT mixtures were studied in the Cr phase and it was found that the electronic conductivities of the intrinsic materials are low due to their large optical band-gaps, low intrinsic mobile carrier concentration and disordered texture in thick (greater than 5 μm) plastic Cr films. Subsequently, the DLCs were doped with the strong electron acceptor F4TCNQ, and it was found that charge transfer between the host and dopant materials leads to changes in light absorption characteristics. The absorption spectra were corroborated with PL spectra and I-V measurements to confirm the formation of a charge transfer complex in the DLC medium, allowing an enhancement of conductivity by two orders of magnitude. All the doped films illustrated vastly improved conductivities, however the 40% HAT6 - 60% HAT10 mixture which exhibited large areas of low birefringence alignment did not translate to the highest measured doped conductivities in out of plane devices, confirming that the alignment is indeed not predominantly homeotropic. Crystalline 5 wt% F4TCNQ doped HAT6 films were found to be less conductive than 0.1 wt% and 1 wt% films, due to scattering and dopant induced disorder. It is hypothesized that this doping mechanism is stable, and conduction is predominantly supported by hole hopping. The results lay the foundation for potential device applications, especially self-assembled DLC hole transport layers for solar cells. This is especially true for the 40:60 HAT6-HAT10 binary mixtures, which were confirmed via AFM to form very smooth spin-coated films. Low temperature melt processing, better control on alignment (1-D aligned molecular wires, rather than amorphous films), and the possibility of further increase in conductivity using combined dopants and different DLC aromatic cores makes F4TCNQ doped DLCs and binary mixtures films promising candidates for future advances in organic electronics.

Acknowledgements

Part of the work was conducted at beam line D1 at the Cornell High Energy Synchrotron Source (CHESS), CHESS is supported by the NSF & NIH/NIGMS via NSF award DMR-1332208. We thank D. Smilgies and X. Sheng for their help during the D1 experiment at CHESS. In addition, the authors would like to thank Dr. Aditya Sadhanala (Department of Physics, University of Cambridge) for help in carrying out PL measurements. We would also like to thank Dr. Abhishek Kumar (Solar Energy Research Institute of Singapore

(SERIS) at NUS) and Prof. Ullrich Steiner (Adolphe Merkle Institute, Fribourg, Switzerland) for insightful discussions and suggestions on the work. J.A.D. is supported by the EPSRC through the Cambridge NanoDTC EP/G037221/1. A.A.K and G.R would like to thank the Cambridge Commonwealth European and International Trust (CCEIT) financial support. A.A.K would also like to thank the Higher Education Commission of Pakistan (HEC) for financial support.

Appendix A. Supplementary data

Supplementary data related to this article can be found at http://dx.doi.org/10.1016/j.orgel.2016.05.027.

References

[1] S. Sergeyev, W. Pisula, Y.H. Geerts, Discotic liquid crystals: a new generation of organic semiconductors, Chem. Soc. Rev. 36 (2007) 1902–1929, http://dx.doi.org/10.1039/b417320c.
[2] R.J. Bushby, O.R. Lozman, Discotic liquid crystals 25 years on, Curr. Opin. Colloid Interface Sci. 7 (2002) 343–354, http://dx.doi.org/10.1016/S1359-0294(02)00085-7.
[3] S. Chandrasekhar, G. Ranganath, Discotic liquid crystals, Rep. Prog. Phys. 57 (1990). http://iopscience.iop.org/0034-4885/53/1/002 (accessed 16.08.14).
[4] N. Boden, R.J. Bushby, J. Clements, Mechanism of quasi-one-dimensional electronic conductivity in discotic liquid crystals, J. Chem. Phys. 98 (1993) 5920, http://dx.doi.org/10.1063/1.464886.
[5] N. Boden, R.J. Bushby, J. Clements, B. Movaghar, Device applications of charge transport in discotic liquid crystals, J. Mater. Chem. 9 (1999) 2081–2086, http://dx.doi.org/10.1039/a903005k.
[6] H.K. Bisoyi, S. Kumar, Discotic nematic liquid crystals: science and technology, Chem. Soc. Rev. 39 (2010) 264–285, http://dx.doi.org/10.1039/b901792p.
[7] Q. Li, Liquid Crystals beyond Displays: Chemistry, Physics, and Applications, John Wiley & Sons, 2012.
[8] B.R. Kaafarani, Discotic liquid crystals for opto-electronic applications † ‡, Chem. Mater 23 (2011) 378–396, http://dx.doi.org/10.1021/cm102117c.
[9] S. Kumar, Discotic liquid crystal-nanoparticle hybrid systems, NPG Asia Mater 6 (2014) e82, http://dx.doi.org/10.1038/am.2013.75.
[10] L. Li, S. Kang, J. Harden, Q. Sun, X. Zhou, L. Dai, et al., Nature inspired light harvesting liquid crystalline porphyrins for organic photovoltaics, Liq. Cryst. 35 (2008) 233–239, http://dx.doi.org/10.1080/02678290701806584.
[11] A.M. de Craats, J.M. Warman, The core-size effect on the mobility of charge in discotic liquid crystalline materials, Adv. Mater 13 (2001) 130–133.
[12] B. Hideo, Organic semiconductors with high conductivity. I. Complexes between polycyclic aromatic hydrocarbons and halogens, Bull. Chem. Soc. Jpn. 29 (1956) 2–7.
[13] M. Pfeiffer, K. Leo, X. Zhou, J. Huang, M. Hofmann, A. Werner, et al., Doped organic semiconductors: physics and application in light emitting diodes, Org. Electron 4 (2003) 89–103, http://dx.doi.org/10.1016/j.orgel.2003.08.004.
[14] L. Schmidt-Mende, a Fechtenkötter, K. Müllen, E. Moons, R.H. Friend, J.D. MacKenzie, Self-organized discotic liquid crystals for high-efficiency organic photovoltaics, Science 293 (2001) 1119–1122, http://dx.doi.org/10.1126/science.293.5532.1119.
[15] Q. Zheng, G. Fang, W. Bai, N. Sun, P. Qin, X. Fan, et al., Efficiency improvement in organic solar cells by inserting a discotic liquid crystal, Sol. Energy Mater. Sol. Cells 95 (2011) 2200–2205, http://dx.doi.org/10.1016/j.solmat.2011.03.024.
[16] Q. Sun, L. Dai, X. Zhou, L. Li, Q. Li, Bilayer- and bulk-heterojunction solar cells using liquid crystalline porphyrins as donors by solution processing, Appl. Phys. Lett. 91 (2007) 10–13, http://dx.doi.org/10.1063/1.2823586.
[17] Y. Yamashita, Organic semiconductors for organic field-effect transistors, Sci. Technol. Adv. Mater 10 (2009) 024313, http://dx.doi.org/10.1088/1468-6996/10/2/024313.
[18] H. Bässler, A. Köhler, Charge transport in organic semiconductors, Top. Curr. Chem. 312 (2012) 1–65, http://dx.doi.org/10.1007/128_2011_218.
[19] C. Destrade, M.C. Mondon, J. Malthete, Hexasubstituted triphenylenes: a new mesomorphic order, Le. J. Phys. Colloq. 40 (1979), http://dx.doi.org/10.1051/jphyscol:1979305. C3-17–C3-21.
[20] X. Zhou, S.-W. Kang, S. Kumar, R.R. Kulkarni, S.Z.D. Cheng, Q. Li, Self-assembly of porphyrin and fullerene supramolecular complex into highly ordered nanostructure by simple thermal annealing, Chem. Mater 20 (2008) 3551–3553.
[21] A.M. Van De Craats, J.M. Warman, Core-size effect on the mobility of charge in discotic liquid crystalline materials, Adv. Mater 13 (2001) 130–133, http://dx.doi.org/10.1002/1521-4095(200101).
[22] N. Boden, R.J. Bushby, J. Clements, B. Movaghar, K.J. Donovan, T. Kreouzis, Mechanism of charge transport in discotic liquid crystals, Phys. Rev. B 52 (1995) 13274–13280, http://dx.doi.org/10.1103/PhysRevB.52.13274.
[23] R. Azumai, M. Ozaki, K. Yoshino, K. Ohta, Electrical and optical properties of discotic liquid crystals with various core structures, in: Proc. 2002 IEEE 14th Int. Conf. Dielectr. Liq. ICDL 2002 (Cat. No.02CH37319), 2002, pp. 397–400, http://dx.doi.org/10.1109/ICDL.2002.1022778.
[24] E.O. Arikainen, N. Boden, R.J. Bushby, J. Clements, B. Movaghar, A. Wood, Effects of side-chain length on the charge transport properties of discotic liquid crystals and their implications for the transport mechanism, J. Mater. Chem. 5 (1995) 2161, http://dx.doi.org/10.1039/jm9950502161.
[25] W.H. Nguyen, C.D. Bailie, E.L. Unger, M.D. McGehee, Enhancing the hole-conductivity of spiro-OMeTAD without oxygen or lithium salts by using spiro(TFSI)2 in perovskite and dye-sensitized solar cells, J. Am. Chem. Soc. 136 (2014) 10996–11001, http://dx.doi.org/10.1021/ja504539w.
[26] A. Abate, T. Leijtens, S. Pathak, J. Teuscher, R. Avolio, M.E. Errico, et al., Lithium salts as “redox active” p-type dopants for organic semiconductors and their impact in solid-state dye-sensitized solar cells, Phys. Chem. Chem. Phys. 15 (2013) 2572–2579, http://dx.doi.org/10.1039/c2cp44397j.
[27] H.J. Snaith, M. Grätzel, Enhanced charge mobility in a molecular hole transporter via addition of redox inactive ionic dopant: implication to dye-sensitized solar cells, Appl. Phys. Lett. 89 (2006) 2004–2007, http://dx.doi.org/10.1063/1.2424552.
[28] C. Krause, R. Zorn, F. Emmerling, J. Falkenhagen, B. Frick, P. Huber, et al., Vibrational density of states of triphenylene based discotic liquid crystals: dependence on the length of the alkyl chain, Phys. Chem. Chem. Phys. 16 (2014) 7324–7333, http://dx.doi.org/10.1039/c3cp55303e.
[29] Q. Li, Self-Organized Organic Semiconductors: From Materials to Device Applications, John Wiley & Sons, 2011. https://books.google.com/books?id=w63h9wiDVWUC&pgis=1.
[30] X.L. Zhou, S.W. Kang, S. Kumar, Q. Li, Self-assembly of discotic liquid crystal porphyrin into more controllable ordered nanostructure mediated by fluorophobic effect, Liq. Cryst. 36 (2009) 269–274, http://dx.doi.org/10.1080/02678290902846611.
[31] E. Pouzet, V. De Cupere, C. Heintz, J.W. Andreasen, D.W. Breiby, M.M. Nielsen, et al., Homeotropic alignment of a discotic liquid crystal induced by a sacrificial layer, J. Phys. Chem. C 113 (2009) 14398–14406, http://dx.doi.org/10.1021/jp9035343.
[32] M.M. Ahmida, S.H. Eichhorn, Measurements and prediction of electronic properties of discotic triphenylenes and phthalocyanines, Trans. E C S Soc. Electrochem. 25 (2010) 1–10.
[33] L.A. Haverkate, M. Zbiri, M.R. Johnson, E. Carter, A. Kotlewski, S. Picken, et al., Electronic and vibronic properties of a discotic liquid-crystal and its charge transfer complex, J. Chem. Phys. 140 (2014) 014903, http://dx.doi.org/10.1063/1.4856815.
[34] N. Boden, Electron transport along molecular stacks in discotic liquid crystals, Mater. Electron. 5 (1994) 83–88.
[35] S. Chandrasekhar, V.S.K. Balagurusamy, Discotic liquid crystals as quasi-one-dimensional electrical conductors, Proc. R. Soc. A Math. Phys. Eng. Sci. 458 (2002) 1783–1794, http://dx.doi.org/10.1098/rspa.2001.0935.
[36] P. Pingel, D. Neher, Comprehensive picture of p-type doping of P3HT with the molecular acceptor F4TCNQ, Phys. Rev. B - Condens. Matter Mater. Phys. 87 (2013) 1–9, http://dx.doi.org/10.1103/PhysRevB.87.115209.
[37] H. Pinto, R. Jones, J.P. Goss, P.R. Briddon, p-type doping of graphene with F4-TCNQ, J. Phys. Condens. Matter 21 (2009) 402001, http://dx.doi.org/10.1088/0953-8984/21/40/402001.
[38] D.-Y. Chen, W.-H. Tseng, S.-P. Liang, C.-I. Wu, C.-W. Hsu, Y. Chi, et al., Application of F4TCNQ doped spiro-MeOTAD in high performance solid state dye sensitized solar cells, Phys. Chem. Chem. Phys. 14 (2012) 11689, http://dx.doi.org/10.1039/c2cp41855j.
[39] Y. Bouligand, Defects and textures of hexagonal discotics, J. Phys. 41 (1980) 1307–1315, http://dx.doi.org/10.1051/jphys:0198000410110130700.
[40] O. Kruglova, E. Mendes, Z. Yildirim, M. Wübbenhorst, F.M. Mulder, J.A. Stride, et al., Structure and dynamics of a discotic liquid-crystalline charge-transfer complex, Chemphyschem 8 (2007) 1338–1344, http://dx.doi.org/10.1002/cphc.200700134.
[41] A.B. Padmaperuma, Substituted molecular p-dopants: a theoretical study, Adv. Mater. Phys. Chem. 02 (2012) 163–172, http://dx.doi.org/10.4236/ampc.2012.23025.
[42] P.N. Murgatroyd, Theory of space-charge-limited current enhanced by Frenkel effect, J. Phys. D. Appl. Phys. 3 (1970) 151, http://dx.doi.org/10.1088/0022-3727/3/2/308.
[43] K. Neumann, M. Thelekkat, Perovskite solar cells involving poly(-tetraphenylbenzidine)s: investigation of hole carrier mobility, doping effects and photovoltaic properties, RSC Adv. 4 (2014) 43550–43559, http://dx.doi.org/10.1039/c4ra05564k.